Supporting Information

Visualizing Fiber End Geometry Effects on Stress Distribution in Composites Using Mechanophores

Nazmul Haque[a], Hao Chun Chang[b], Chia-Chih Chang[b], Chelsea S. Davis[a,c,d]*

[a]School of Materials Engineering, Purdue University, West Lafayette, IN, 47906 USA

[b]National Yang Ming Chiao Tung University, Taiwan

[c]Department of Mechanical Engineering, University of Delaware, Newark, DE, 19716 USA

[d]Department of Materials Science and Engineering, University of Delaware, Newark, DE, 19716 USA

*Corresponding Author: Email address: chelsead@udel.edu (C.S.D.)

1. Load-Displacement Plots for Different Fiber Ends

The load vs. displacement curves for each fiber end geometry—round, cone, sharp, and flat—illustrate the load-bearing behavior observed during single fiber pull-out tests. Multiple tests are shown for each geometry, demonstrating the consistency and repeatability of the measurements. The peak load and displacement vary across fiber shapes, indicating differences in interfacial stress transfer and failure mechanisms.

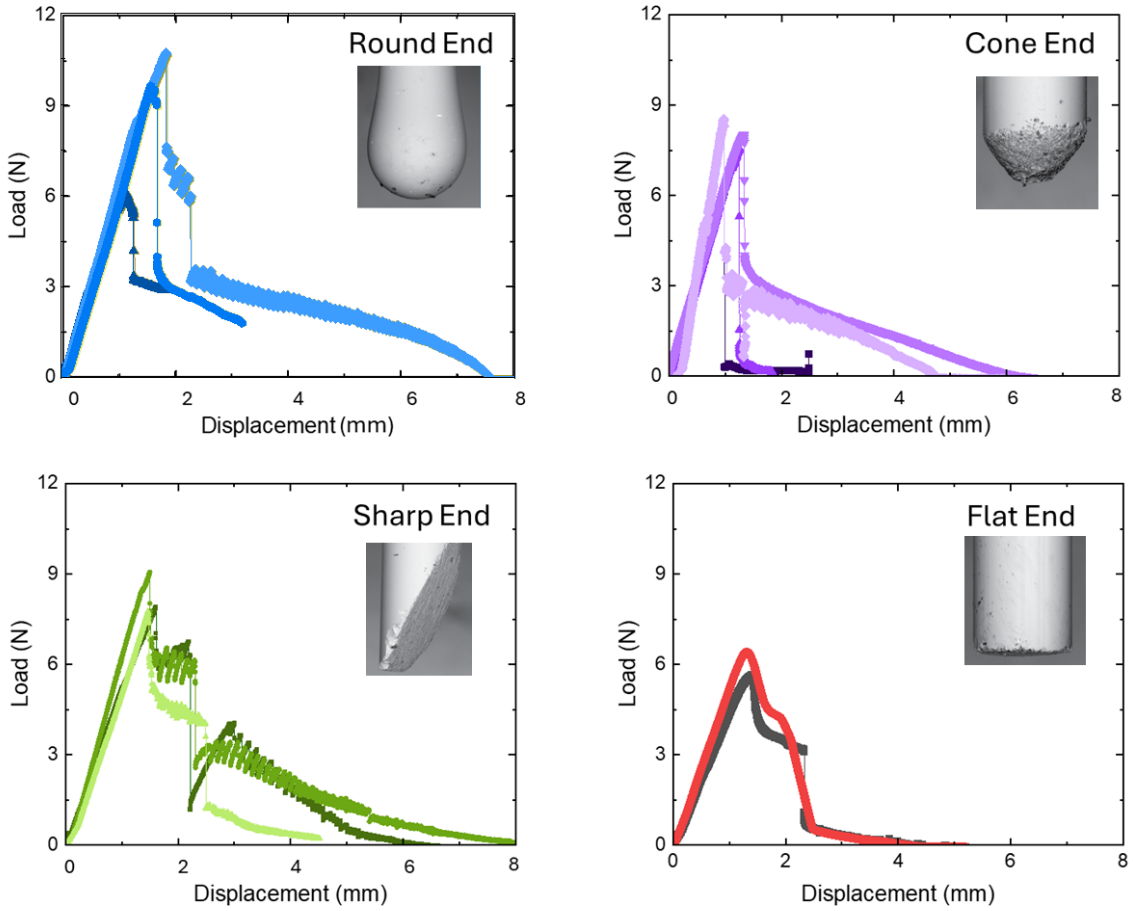

Fig S1: Load vs. displacement curves for various fiber end geometries (round, cone, sharp, flat) obtained from single fiber pull-out tests. Each plot includes multiple test runs to show consistency. SEM images in insets show fiber geometry (diameter of each fiber 300 ± 2 μm).

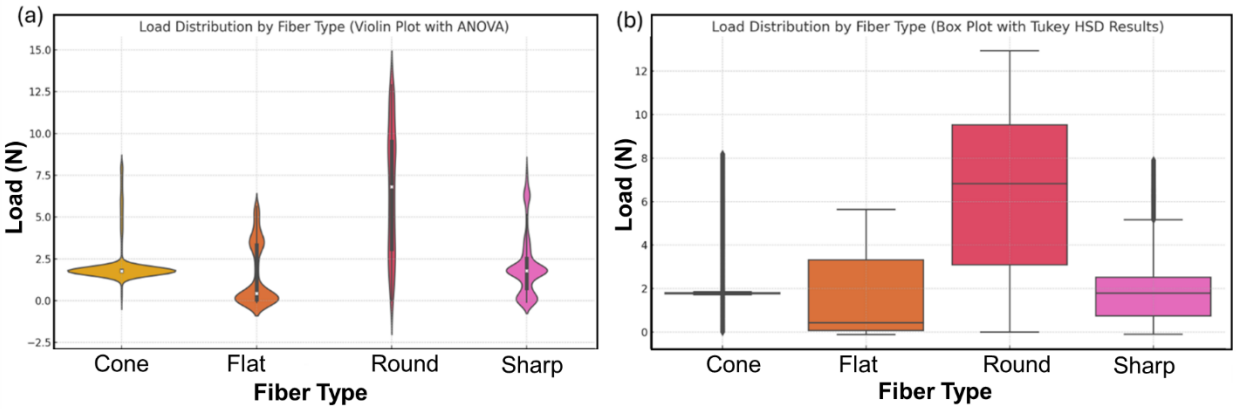

Fig S2: (a) Violin Plot with ANOVA showing load distribution for each fiber geometry. (b) Box Plot with Tukey HSD Analysis provides pairwise comparisons.

The violin plot with Analysis of Variance (ANOVA) illustrates load distribution within each geometry, confirming through statistical testing that these differences are significant. The box plot with Tukey Honestly Significant Difference (HSD) analysis provides a detailed comparison of load values, identifying which fiber pairs differ significantly in their mean load. Together, these plots offer a comprehensive view of how fiber end geometry influences both peak load capacity and consistency.

2. Mechanophore (MP) Activation at Different Fiber Ends

The comparison of MP activation for different fiber end geometry highlights the sensitivity of this method, offering insights into the localized stress fields and the mechanical performance of the composite under different conditions. As the fiber is pulled out of the matrix, the intensity of mechanophore (MP) activation varies with each fiber end geometry, reflecting the different stress distributions and failure mechanisms. Initially, as the stress increases, we observe the initiation of cavitation near the fiber tip, which is more pronounced in sharp and cone-shaped ends due to the sharp features of these tips that localize and concentrate stress. This cavitation marks the onset of

debonding, leading to a gradual increase in MP activation. As the displacement progresses, the stress intensifies further, ultimately causing the fracture of the matrix at the fiber tip.

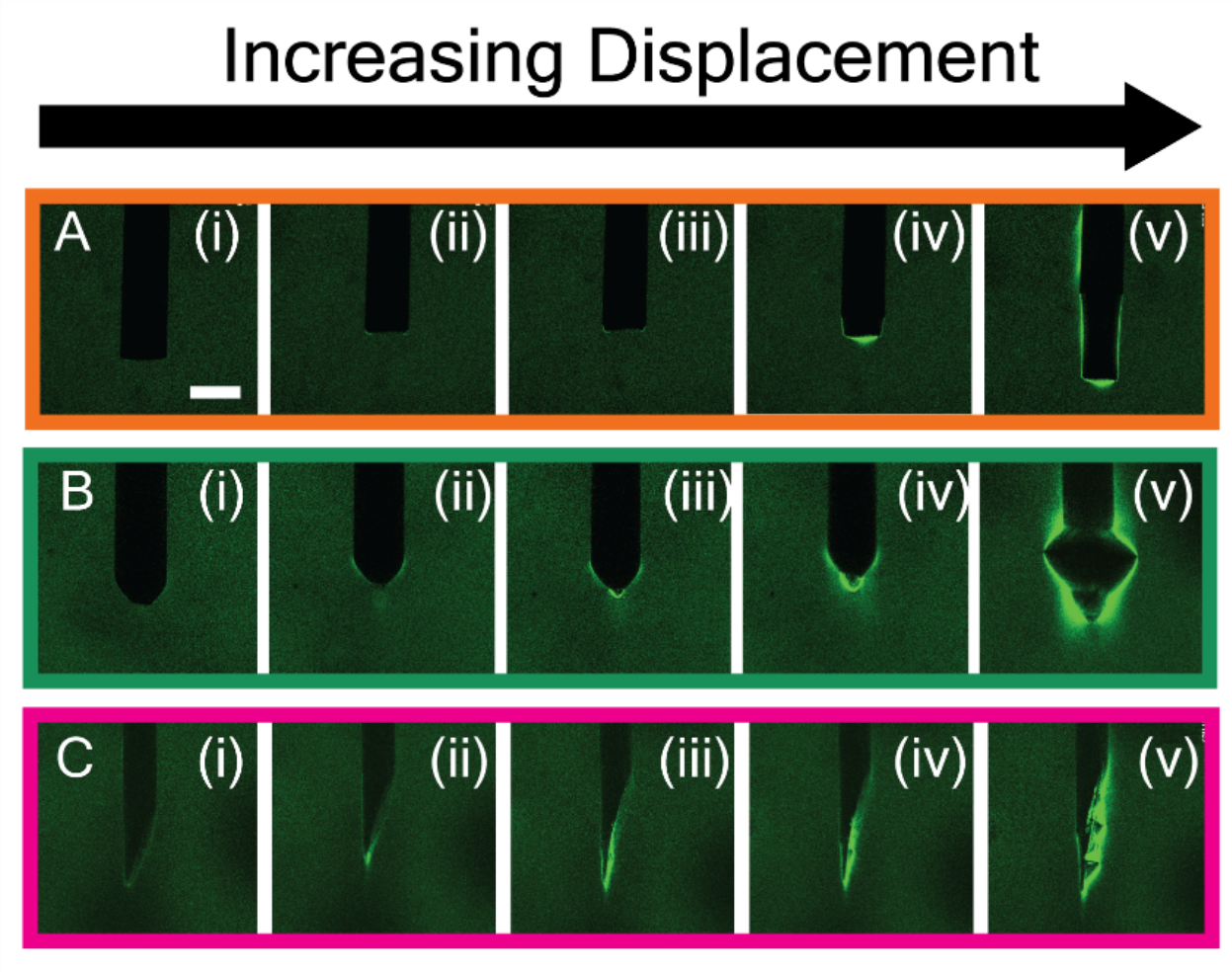

Fig S3. Visualization of mechanophore (MP) activation during fiber pull-out tests for different fiber end geometries: (A) flat end, (B) cone, and (C) sharp end. Each fiber end case includes an image sequence (i-v) that captures different stages of pull-out displacement, corresponding to the progressive activation of MPs. These sequences illustrate how the MP activation varies with the geometry, reflecting differences in stress distribution and fracture behavior. The scale bar shown in (A-i) represents 300 μm and applies to all images.

The figure S4 shows raw intensity measurements as a function of distance from the fiber tip for four different fiber end geometries: round, cone, flat, and sharp. Each plot illustrates how fluorescence intensity, indicating stress distribution, varies along the distance from the fiber tip.

The differences in intensity profiles reflect the influence of fiber end geometry on stress localization within the composite material.

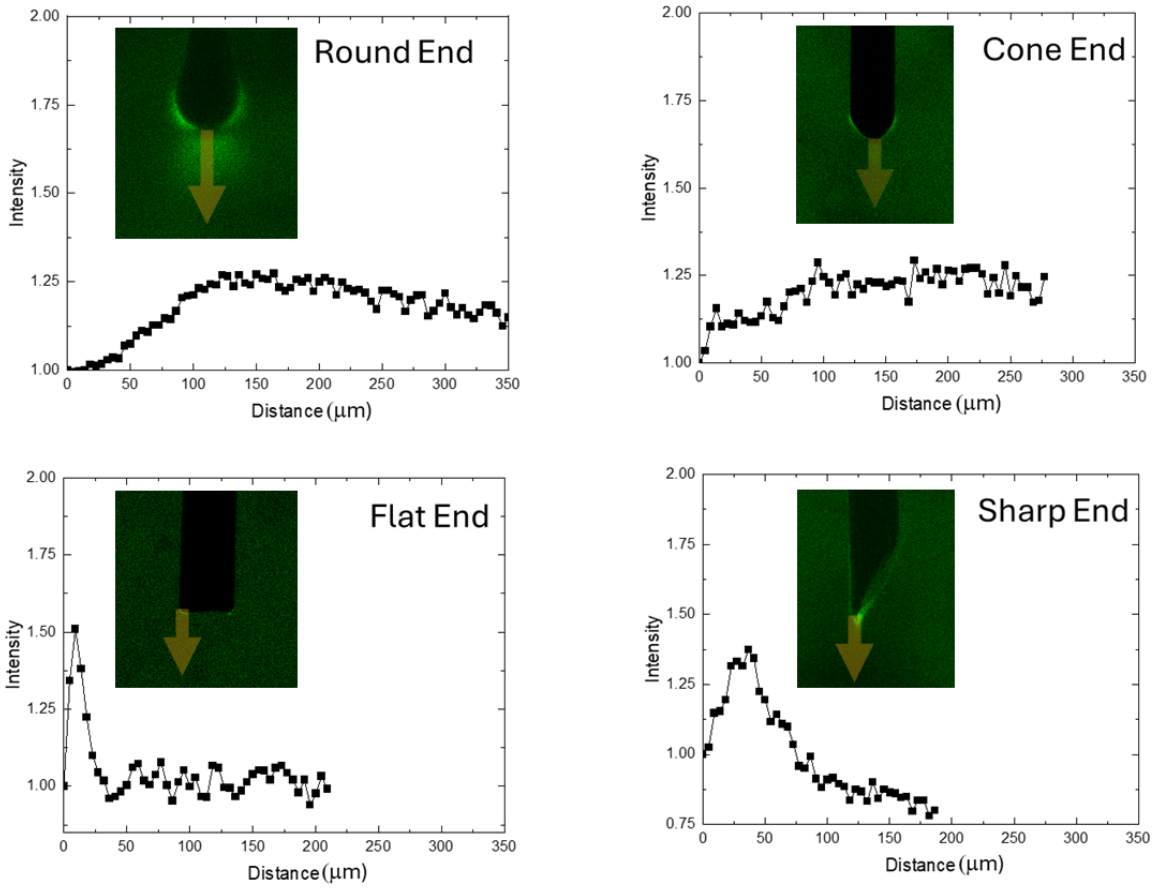

Fig S4. Raw intensity measurements as a function of distance from fiber tips with different geometries (round, cone, flat, sharp fiber ends). Yellow arrows in insets indicate location of trace.

Table 1 presents the maximum load each fiber end geometry (round, sharp, cone, and flat) can withstand, along with the distance from the fiber tip where peak intensity is first detectable. The round end exhibits the highest load capacity, followed by cone, sharp, and flat, indicating variations in strength and structural performance influenced by geometry. The distance values

highlight the stress distribution across each fiber type, showing how end geometry affects both load-bearing capacity and the initiation point of maximum stress.

Table S1: Summary of load-bearing characteristics and maximum intensity and stress occurring distances from the tip surface for different fiber end geometries.

Fiber end type	Max. load (N)	Distance of peak intensity from tip surface (μm)
Round	11.5	125
Sharp	9	40
Cone	8.5	100
Flat	5.6	10

3. Finite Element Analysis (FEA) and Stress Comparison Across Different Fiber Ends

Finite element analysis (FEA) was employed to model stress distribution around various fiber end geometries during the fiber pull-out process. The simulation treats both the fiber and matrix as solid and deformable materials, allowing for detailed analysis of how different fiber shapes—round, cone, flat, and sharp—affect stress distribution in the matrix.

The FEA was conducted in Abaqus with the PDMS matrix characterized by the Ogden hyperelastic model to simulate its large-strain response accurately. We used a second-order Ogden model with constants derived from experimental stress-strain data: μ_1=0.4095 MPa, μ_2=0.0243 MPa, α_1=1.11, and α_2=−6.19, which captures the non-linear mechanical response of PDMS under tension. The FEA model is a 2D axisymmetric setup with matrix dimensions of 3.5 mm in width by 14 mm in height, simulating the experimental setup for pull-out tests with an embedded fiber length of 7 mm. The fiber, modeled as an elastic material with a Young's modulus of 70 GPa and Poisson's ratio of 0.3, was subjected to a displacement-controlled load at the top with maximum

displacement of 7 mm, while the matrix bottom was fixed to replicate the fixed-bottom boundary condition used experimentally. The fiber-matrix interface was modeled as perfectly bonded (no interfacial slip) to align with observations of strong adhesion in PDMS-fiber systems under our test conditions. We used a refined quadrilateral mesh with hybrid axisymmetric stress elements (CAX4RH). Mesh refinement was implemented at the fiber-matrix interface and the immediate surrounding regions, with elements as small as 5 µm at the fiber end, ensuring adequate resolution for capturing stress gradients and mechanophore activation zones. This fine meshing at the interface improves the model's accuracy in simulating localized stress concentrations around various fiber end shapes, aligning the FEA results closely with observed fluorescence intensity variations.

The stress to intensity calibration has been carried out following established protocol described in our previous work [1–3]. Comparison of stress distributions for different fiber ends confirm that the calibration method accurately predicts stress profiles for more complex fiber geometries, including sharp ends, demonstrating its robustness for developing calibrated stress profiles across various fiber end shapes.

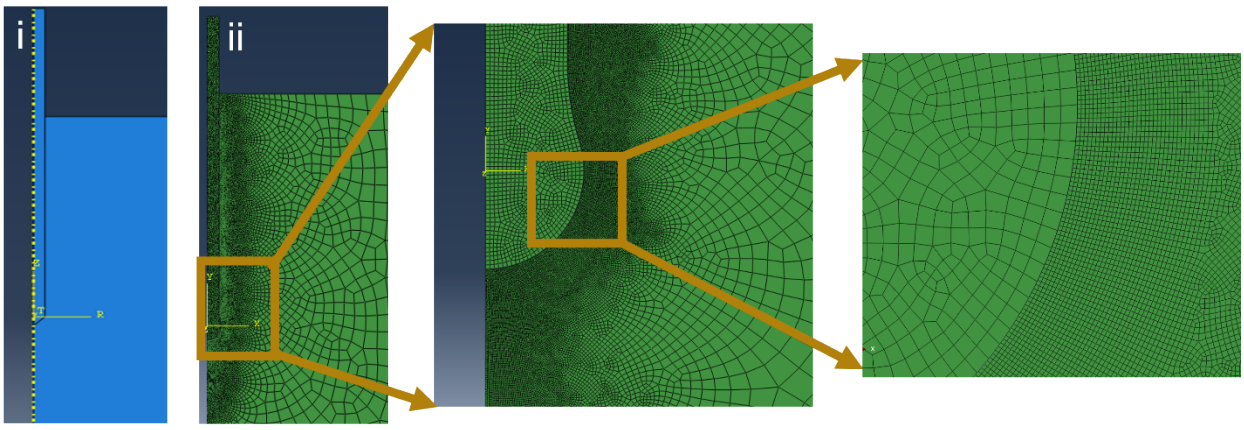

Fig S5. Configuration and meshing details of the finite element analysis (FEA) model. (i) The model illustrates an axisymmetric single fiber setup, depicted as a 2D cross-section at the mid-plane of the sample, with matrix dimensions of 3.5 mm by 14 mm and a fiber radius of 150 µm, embedded 7 mm into the matrix. (ii) A quadrilateral mesh was used, featuring a standard quadratic

hybrid formulation within the axisymmetric stress family of elements. A finer mesh was applied at the fiber-matrix interface (shown in the zoomed-in view) to capture precise interactions in this critical region.

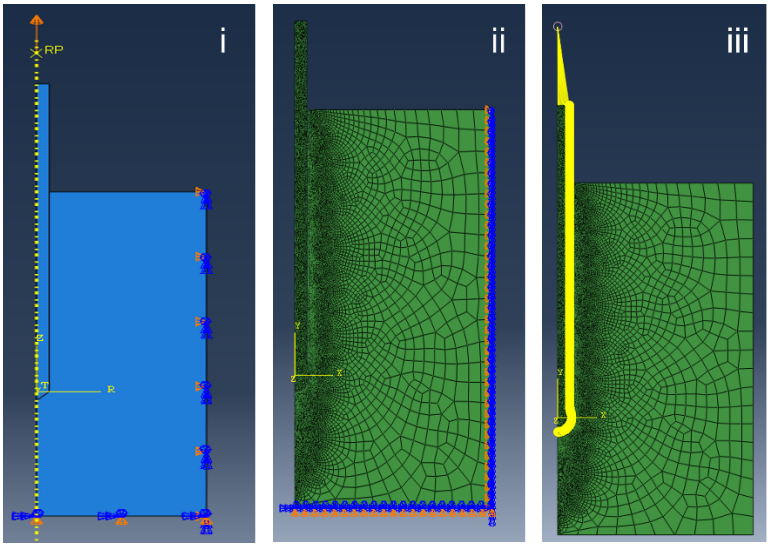

Fig S6. Boundary conditions applied for model simplification. (i) Symmetry conditions were imposed, fixing movement along the x-axis for the right surface and along the y-axis for the bottom surface. A displacement boundary condition was applied to the fiber top surface to simulate uniaxial tensile strain. (ii-iii) Meshed profiles with boundary conditions. The fiber and matrix were tied together, with the matrix designated as the secondary surface. A kinematic coupling interaction was established between the fiber's top surface and a reference point to track load displacement. Mesh refinement was used to improve simulation accuracy while minimizing the number of elements and computational cost.

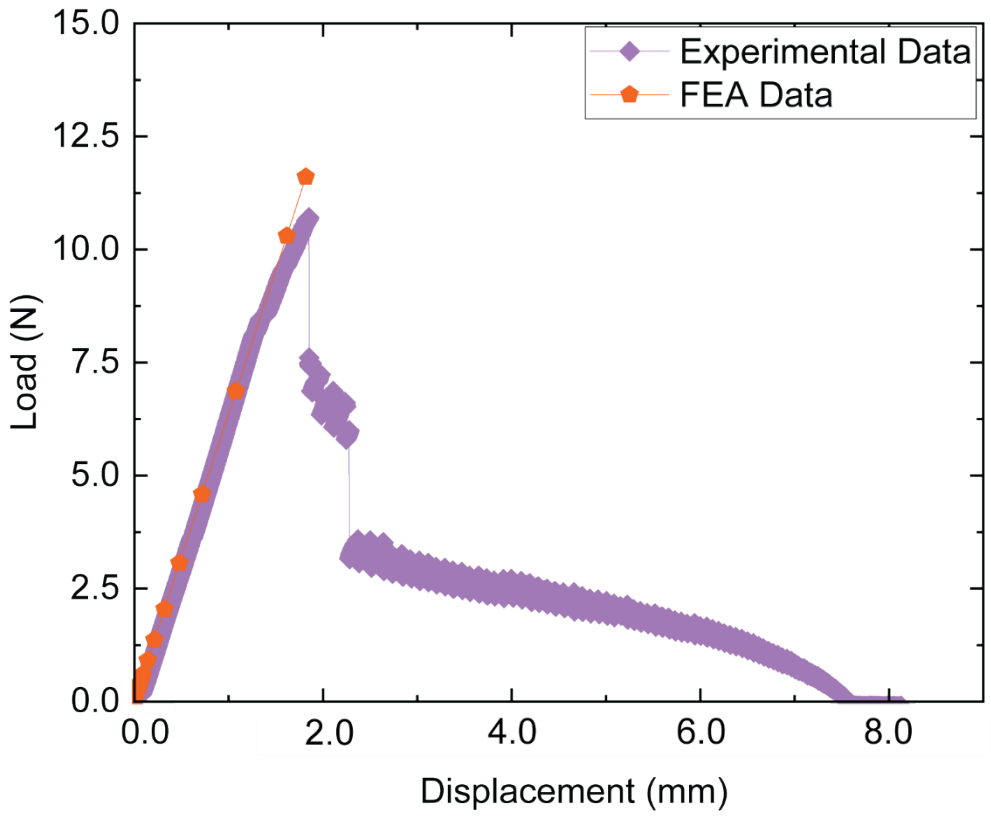

Fig S7. Comparison of fiber pull-out load versus displacement obtained from both experimental data and finite element analysis (FEA) using round fiber end geometry. The plot shows a strong correlation between the experimental and FEA results up to the linear regime, confirming the accuracy of the model in predicting the initial mechanical response. The close agreement in the initial phase underscores the model's reliability in simulating the early stages of fiber-matrix mechanical deformation.

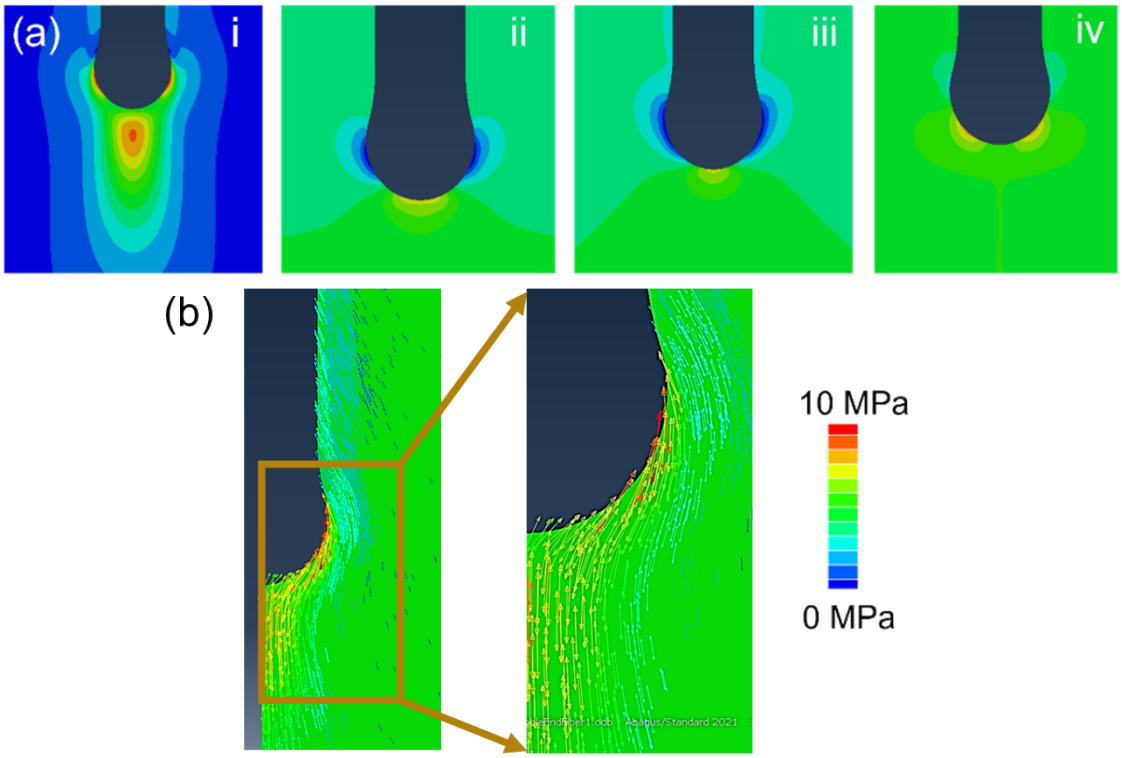

Fig S8. Comparison of stress responses for various stress descriptors and the directionality of maximum principal stress. (a) Analysis of different stress descriptors: (i) Stresses parallel to the loading direction, including the depletion zone observed in experiments. (ii) In-plane stresses orthogonal to the loading direction. (iii) Out-of-plane stresses orthogonal to the loading direction. (iv) In-plane shear stresses. (b) Directionality of maximum principal stress, illustrating the stress distribution magnitude around the matrix at the round fiber tip. The color code applies to all the images.

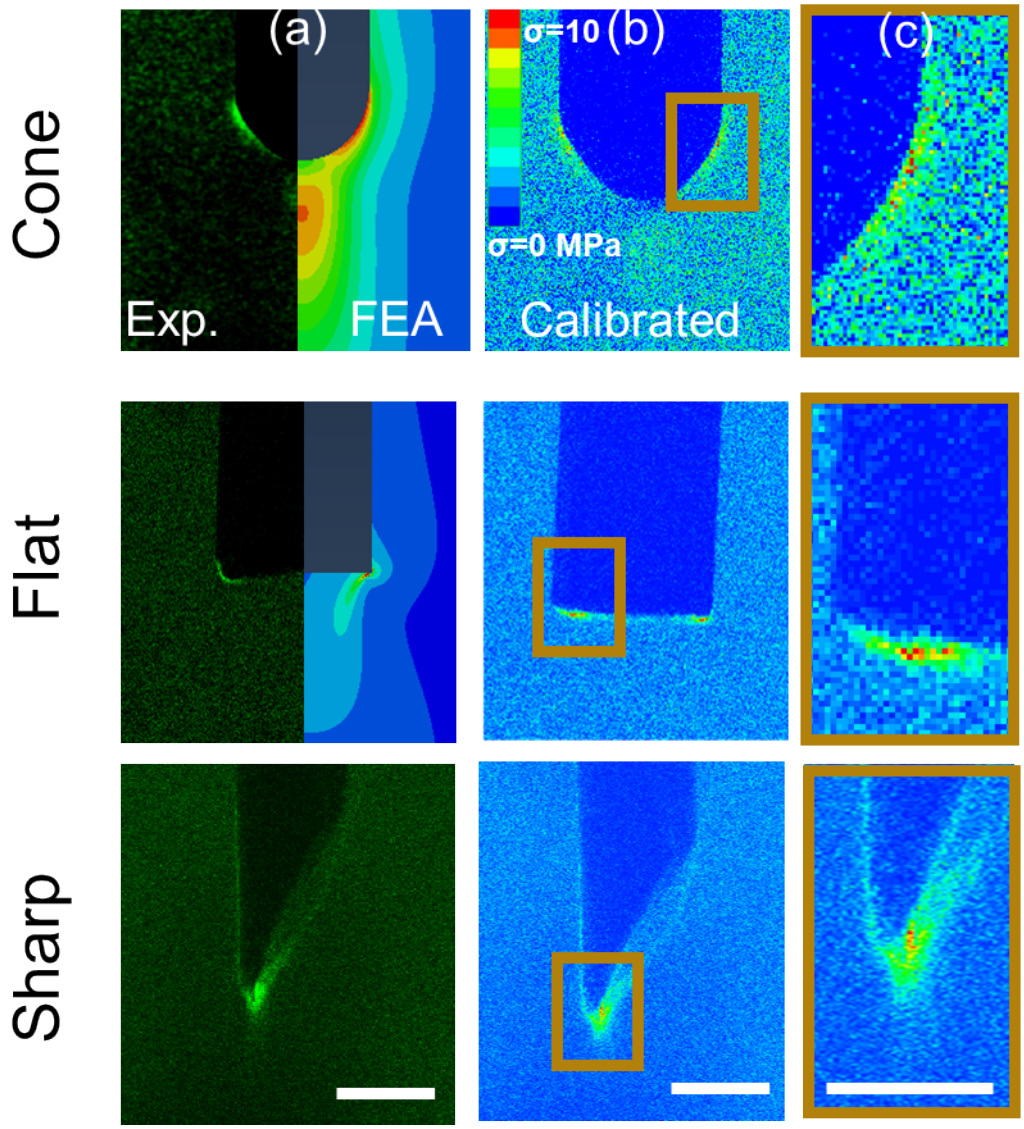

Fig S9. Stress distributions from finite element analysis (FEA) have been compared with experimental intensity measurements for flat and cone fiber ends, using the calibration developed for round fiber ends. This comparison confirms that the calibration method accurately predicts stress profiles for more complex fiber geometries, including sharp ends, demonstrating its robustness for developing calibrated stress profiles across various fiber shapes. The color code applies to all the images. Scale bars in columns a, and b represent 300 μm and c represents 100 μm and apply to all images in the respective columns.

4. References:

[1] J.A. Gohl, T.J. Wiley, H.-C. Chang, C. Chang, C.S. Davis, Stress quantification in a composite matrix via mechanophores, Front. Soft Matter. 3 (2023) 1–10. https://doi.org/10.3389/frsfm.2023.1125163.

[2] N. Haque, J. Gohl, C. Chang, H.C. Chang, C.S. Davis, Quantifying Localized Stresses in the Matrix of a Fiber-Reinforced Composite via Mechanophores, Macromol. Chem. Phys. 224 (2023) 2300298. https://doi.org/10.1002/macp.202300298.

[3] M.L. Rencheck, B.T. Mackey, Y.Y. Hu, C.C. Chang, M.D. Sangid, C.S. Davis, Identifying Internal Stresses during Mechanophore Activation, Adv. Eng. Mater. 2101080 (2021) 1–10. https://doi.org/10.1002/adem.202101080.